SFSA Cast in Steel 2026 - Horseman's Ax Technical Report

Michigan Technological University - Axes and O's

Team Members:

Daniel Branagan

Nicholas Joerin

Rachael Roszman

John Bellmann

Chase Henderson

Advisors:

Dr. Caleb Stetson

Industry Partner:

Aalberts Surface Technology - Dr. Kathy Hayrynen

Executive Summary

SFSA has created this competition to encourage students to learn about making steel products using the casting process and applying the latest technology available. In this work, a horseman's ax was designed and produced using austempered ductile iron (ADI) to take advantage of its high strength, toughness, and castability. Two design approaches—an integrally cast handle and a separate wooden handle—were developed and evaluated. The final casting and heat treatment process produced components with suitable mechanical properties and geometry for competition requirements while demonstrating the advantages of ADI in complex cast applications.

Historical background

In the 15th and 16th centuries, armor became increasingly prevalent on the battlefields of Europe to the point where even regular soldiers had access to armor. Bladed weapons such as swords proved less effective in this environment, while projectile weapons, blunt edges and pointed weapons capable of piercing armor become increasingly prevalent. These blunt weapons excelled at damaging armored opponents. The horseman's ax has a unique niche which allows for extreme versatility against armored or unarmored opponents. The horseman's ax was often viewed as a secondary weapon because of its relatively small size and thin profile allowed it to hang conveniently on a belt. The blade was not typically razor sharp, as it was not primarily used for piercing armor and excessive sharpness could lead to edge fracture or curling. The piercing tip on the back of the ax was used to penetrate armor while the blade could cause severe blunt force trauma on armored opponents. The ax could also be used to pull an opponent off his horse by hooking on to the opponent's armor. There is significant variation in size of the spike present on horseman's axes. Some horseman axes have large or small spear points at the top of the ax. However, this varied by region and time period and was not a defining feature.

The weight and dimensions of historical horseman's axes are given in Appendix A and were used as a reference for the design in this work.

Material Selection

At the 2025 Cast in Steel competition, our team met with Dr. Kathy Hayrynen, an expert in austempered ductile iron, and discussed the potential for ADI to compete against cast steel. For applications that do not require an extremely sharp edge, ADI performs well. When the horseman's ax competition was announced, ADI was selected as a material for the 2026 Cast in Steel competition.

Austempered Ductile Iron Performance

Austempered ductile iron (ADI) is a special grade of ductile cast iron which has undergone a complex heat treatment. Components requiring high strength, fatigue resistance, and

toughness are commonly made from ADI in industries such as agriculture, mining, automotive and locomotive[1].

In addition to its high strength, ADI is also 10% less dense than steel[2] owing to the large volume fraction (~10%) of graphite which has a low density. This is accompanied by significantly reduced shrinkage (due to graphite expansion upon cooling) and extremely high fluidity[3] due to its high silicon content. These properties allow ADI to be cast in complex geometries with minimal defects.

For the production of a cast horseman's ax, this material is capable of producing a complex geometry while maintaining good properties. This application is especially well suited for ADI since a horseman's ax does not need to maintain a razor sharp edge which would favor a high strength steel. In this case, toughness is the crucial property which ADI excels at, not only because of its intrinsic toughness, but also its ability to reduce shrinkage during solidification.

Mechanical Design and Theme

A historical ax from the 1500s was used to produce a faithful rendition. An aesthetic theme was chosen to utilize the versatility of the casting process. The high fluidity and low shrinkage of cast iron allowed for significant design freedom. A heart theme was selected in accordance with the team name "Axes and O's" providing a strong aesthetic motif to accent the functional parts of the axes.

A key design decision was whether to cast a metal handle or only the head. Historical examples exist for both wood and metal handles, each with distinct advantages. Rather than selecting a single approach, both handled and handle-less versions were produced. This enabled evaluation of two unique designs but required two separate patterns.

For each iteration, a 3D-printed CAD model was used to evaluate feel and ergonomics. These physical evaluations directly informed design adjustments, ensuring the final ax felt comfortable and well-balanced in hand.

Handled

The initial handled ax design was a close copy of the reference ax. Additional geometric complexity was added to better utilize the casting process. A thin heart-shaped frame was added on the outside of the ax. This increased complexity while making the ax more visually distinct. These sections also provide functional benefits, bearing some load and acting as a hook allowing the ax to be easily carried on a belt, which is crucial for its use as a secondary weapon.

The second iteration of the ax design removed significant weight from the ax head while adding some additional aesthetic details in the form of heart-shaped protrusions. The pick was also curved downward slightly as is historically common and improves alignment with the target

[1] W. Smith, Structure and Properties of Engineering Alloys, 2nd ed. McGraw-Hill, 1993.
[2] H. Krawiec, J. Lelito, M. Mróz, and M. Radoń, "Influence of Heat Treatment Parameters of Austempered Ductile Iron on the Microstructure, Corrosion and Tribological Properties," Materials, vol. 16, no. 11, p. 4107, May 2023, doi: 10.3390/ma16114107.
[3] J. G. Sylvia, Cast Metals Technology. Addison-Wesley Publishing Company, 1972.

during a swing. The handle was extended and some small rondles were added to assist with securing a handle. Additionally a heart ornament was added at the bottom of the handle primarily as an aesthetic feature; however, it may also act as a bludgeon.

The final ax design saw a few small but notable changes (Figure 1). The most significant change was a reduction in handle length. This change was made because the 3D-printed second design felt unwieldy, a 3-inch reduction significantly improved handling. The pick length was reduced while increasing the cross section to increase the strength. Minor aesthetic changes included shaping the top rondle into a heart and making the bottom heart more prominent.

Handle-less

The design of the handle-less ax mirrored that of the handled version (Figure 2) with both the heart-shaped frame and pick features from the handled ax. In the handle-less version, features on the pick and blade were made as indentations rather than protrusions, since this reduced weight while having limited impact on strength. Fillets were added where the heart-shaped frame intersected the ax body, improving castability and pattern removal from the mold.

A 3D printed version of the initial handle-less ax head felt too large, particularly the length between the pick and the blade. As a result, the ax was shortened from 9.75” to 8.5”. The heart-shaped frame length was kept constant, increasing the openings between the handle and pick. This improved pattern removal and allowed better sand packing during mold making

Casting design and patternmaking

Handled Casting Design

The initial handled ax gating system was designed to improve casting by placing the sprue near the end of the mold; the ax was mirrored across the center line for simplicity. The runner was stepped at each gate to maintain the head pressure and reduce the total cast metal. In the second design iteration, the sprue was centered and the ax was rotated 180 degrees about the center of the mold instead of mirrored. The final revision consolidated the axes toward the center while modifying the runner to reduce footprint and excess metal.

Simulations performed on the V1 and V2 designs showed that V2 had virtually no shrinkage or porosity. The V3 design was very similar, and the only major change was a reduction in gate length which lowered the overall mold weight (Figure 3).

The runner was designed to accommodate available 1 inch circular cast iron filters while maximizing the ease of casting. The initial runner was 1 inch wide with a maximum thickness of 1.2 inches, and the sprue was placed near the ax head. The gating and runner were designed in order to maintain constant pressure throughout the runner, which was accomplished by decreasing the area of the runner along its length. The runner height was calculated with the Equation 1, where RH_n is the runner height after the nth gate, RA_{n-1} is the runner area before the nth runner, GW is the gate width, and RW is the runner width:

$$RH_n = \frac{RA_{n-1} - 2GW}{RW} \quad \text{(Equation 1)}$$

The maximum thickness was adjusted until there was sufficient material left after the final gate to create a sand trap at the end of the runner. This method was used on all other versions to calculate the runner height along the length of the runner.

Before 3D printing, a 3% draft was added to all surfaces to assist with mold making. The final design was then 3D printed out of ABS plastic using a Creality K1C 3D printer. Pin holes were designed into the 3D printed parts to aid in aligning the parts on both sides of the matchplate. Due to bed size limitations, the design was sliced into smaller printable parts, which were assembled onto a wooden matchplate once they had been printed. Two indexing pins were added to opposite corners of the pattern to aid in alignment of the two mold halves. During the design process, it was found that sand could be saved by rotating the pattern on the matchplate about 20 degrees (Figure 4). The cope and drag sides of the final handled ax assembly are shown in Figure 5.

Handle-less Casting Design

There were a number of design iterations for the handle-less ax, but a vertically parted mold was determined to be the most effective. Initially, the casting was designed with the axes oriented horizontally, but this was changed in favor of a vertical tilted design. InspireCast simulations showed no real issues with casting any of the designs, so a design was chosen that minimized metal and sand usage. This design reduced the total mold size as well as the weight of metal required for filling the mold. The design iterations are shown in Figure 6, where V4 is the final design.

In order to attach a handle, a core was designed to keep the eye of the ax from being filled with metal. A separate core box was also designed based on this model. In the final phases of the design, we realized that this design was mirrored across the sprue; this meant that we could make two identical mold halves and put them together for the final mold assembly. To do this, a plate was added to the CAD model which allowed an indexing hole to be added to one side and a matching protrusion to the other side. The remaining parts were glued onto ABS plates of the same thickness. Prior to printing, all surfaces were drafted to 3 degrees to assist with mold making. This was then mounted onto an existing mold box for patternmaking. The final CAD and final pattern is shown in Figure 7.

Mold Making

No-bake resin bonded sand was used to make molds and cores due to its ability to produce high surface quality and to retain fine details and small surface features on cast parts. However, no-bake molds have a lower permeability than green sand molds, meaning that it was crucial to ensure that the molds were properly vented.

Four molds were made for each of the two patterns, allowing 8 handled axes and 8 handle-less axes to be cast. Once parting dust had been added to the pattern and mold box, sand was packed onto the pattern to fill the mold box. The sand was allowed 10 minutes to cure, and after this time had passed, the mold was carefully removed from the pattern and mold box.

In the gaps between the ax-head and shaft of the handled ax, sand tended to break off the mold and stick to the pattern. This sand was carefully removed from the pattern and glued back onto the mold. The vertically parted molds for the handle-less ax used a standard mold box in the MTU foundry. Unlike with the handled ax, sand did not stick to the pattern, likely due to the presence of fillets on the frame of the handle-less ax where there were none on the handled version.

A core was necessary to cast the hole for inserting the wooden handle on the handle-less ax head. To make the cores, a 3D printed core box was clamped together and filled with no-bake sand. Once the sand had cured, the core was removed from the box and filed down to fit well in the mold. The mold was blown out, the cores and a filter were inserted, and the two halves were glued together to minimize the amount of loose sand in the mold.

For both molds, the filters were larger than the slot in the mold, meaning that manual expansion of the filter holes was necessary. In addition, the alignment pins were shaved down slightly to ensure that they would fit in the holes on the opposite half of the mold, allowing the two halves of the mold to come together properly.

To reduce the time spent fettling the axes, defects in the molds were manually removed, especially ridges in the mold where the pins were located on the pattern and ridges or grooves at the joints between 3D printed pattern pieces. Vents were drilled in the cope, a filter was inserted, and the molds were blown out before being glued together to eliminate as much loose sand from the inside of the mold as possible. Finished molds are shown in Figure 8.

Casting

Charge weighing

Prior to casting, charges were weighed out using the raw materials the foundry had on hand. The charge sheet used is given in Appendix C. While the majority of raw material could be added directly to the furnace, the magnesium treatment and topsteed was kept separate to be added to the ladle rather than the melting furnace.

Pouring

An induction furnace was used for melting the metal; the primary additions were steel punchings and ductile iron riser returns from an industrial foundry. The 50 lbs induction furnace is shown in Figure 9.

Unfortunately, the metallic copper additions were not added, causing the copper target to be undershot. While the iron was melted, the ladle was heated using a natural gas jet; this ensured that the molten metal would not solidify in the ladle during the magnesium reaction. The ladle heater is shown in Figure 10.

Immediately prior to pouring, the ladle was removed from the heater and set upright. Then, topseed, powdered magnesium ferrosilicate, and steel punchings were added in that order to the bottom of the ladle, and a lid was added that partially covered the top. The ladle was then brought to the melting furnace and molten metal was poured into the ladle. The molten metal

immediately began to react with the magnesium. The lid was kept on the ladle for around 1 minute to give the magnesium reaction time to complete. Two handle-less molds and two handled molds were then poured.

Following the first heat, a second heat was done in the exact same way. The castings were broken from the molds approximately 1 hour after casting. Three out of four handless molds broke out during casting due to improper mating between the two halves. None of the handled molds failed, although one of them only partially filled because the ladle ran out of metal.

The castings produced are shown in Figure 11.

Fettling

After breakout, the axes underwent multiple rounds of fettling in order to refine the overall shape of the axes and define the smaller details. Larger excess material sections were removed through use of a hammer and cut-off saw. Detail-work was achieved through use of diamond tipped rotary bits. An example before-and-after of this process is shown in Figure 12.

Material qualification before heat treatment

Prior to heat treatment, the material needed to be characterized to ensure that only the best axes would be sent to Aalberts for heat treatment. Visual inspection of the castings showed 4 handled axes were in a very good condition, with only some minor aesthetic cold shuts. Only one mold of handle-less axes produced a full casting and both of these axes were in excellent condition with no visual defects. Microstructural characterization was performed in order to ensure that the material would be suitable for the austempering treatment. If no axes passed the microstructural characterization, new castings would have to be made.

As-cast microstructural characterization

As-cast ductile iron contains 3 phases: ferrite (the primarily iron phase), cementite (iron-carbide Fe_3C) and spherical graphite (the most stable allotrope of carbon). For qualification of ductile iron meant for ADI heat treatment, the most crucial factor is the nodularity of the graphite. Nodularity is a measure of roundness of graphite nodules. This factor is crucial because graphite acts as a stress concentration, if the graphite is not round this stress concentration will be dramatically increased.

Nodularity measurements were performed on small samples of cast iron taken from the in-gate of the axes. This section was mounted in bakelite and polished to 3µm. Images were taken using a metallurgical microscope and images were analyzed using ImageJ and manual thresholding as well as ChatGpt (v5.2). An example of the polished surface is given in Figure 13 along with the thresholded image.

Nodularity was measured using circularity values via ImageJ's analyze particles feature. Nodularity was evaluated as the area of graphite having circularity greater than 0.65 divided by total graphite area; volume fraction and average graphite diameter was also calculated. Values

were verified using ChatGPT V5.2; the prompt given to ChatGPT is given in Appendix D. The tabulated values are given with their 95% confidence limit in Table 1.

Analysis of the graphite shows that both casting B and the handle-less ax had very good >90% nodularity. Casting A had lower nodularity as measured by ImageJ and ChatGPT; a nodularity less than 80% is considered insufficient for producing high-grade ADI and therefore only the B castings and handle-less axes would be sent for heat treatment.

An interesting metallurgical note is that the handle-less ax has a smaller graphite fraction and smaller graphite radius, this is not due to a difference in chemical composition; rather it is because the handle-less mold was physically smaller. The smaller size of the mold increased the cooling rate which reduces the amount of time carbon had to diffuse into the graphite. This can be easily seen on the etched samples where the ferrite rings surrounding the graphite nodules are larger in the handled ax. The etched microstructures of the B handled and handle-less axes are shown in Figure 14.

Chemical composition was characterized by using optical emission spectroscopy (OES) which is reasonably accurate for all elements but will provide an under-estimation of carbon concentration due to carbon being present in highly stable graphite. The chemical composition of handled B and handle-less axes from OES are given in Table 2.

Comparing the target chemical composition to the measured composition shows that the axes were high on Si, very low on Cu and on target with Mn, P and Sn. OES does not accurately measure carbon when graphite is present and based on the microstructure we are on target. The actual Mg concentration is not a real concern since it is only added to nodularize the graphite.

While the copper content is lower than the target, this is not anticipated to affect mechanical properties because copper is primarily added to cast iron to stabilize pearlite. For larger castings, this is a crucial role as carbon will quickly diffuse to the graphite which will leave very little free carbon for autempering. Since our casting has thin sections, there is a significant pearlite fraction retained in the as-cast microstructure so this material is extremely well suited for austempering treatment.

Heat Treatment

The austempering process is a complex heat treatment requiring specialized equipment. For this process, the team worked with Aalberts' Oshkosh facility, which specializes in austempering cast iron and steels. Aalberts' process uses specialized furnaces which maintain a carburizing atmosphere to ensure that the surface of the cast iron will not be decarburized. Additionally, their specialized molten salt quench tanks are essential for the heat treatment of ADI.

A grade 3 ADI heat treatment was selected, which provides a good balance of strength and toughness. This grade has an approximate tensile strength of 1200 Mpa (175 Ksi), 4% elongation and a charpy impact toughness of 60 Joules[4].

[4] "Austempered Ductile Iron ASTM A897 ADI Grade 1200 / 175 (Grade 3) - Carson Castings." Accessed: Mar. 25, 2026. [Online]. Available: https://www.foundry-source.com/austempered-ductile-iron-grade-3

The heat treatment of ADI uses a 3 step process: the first step is austenitizing, then the material is quenched to a temperature above the martensite start (M_s) temperature, then it is held at that temperature until the completion of austempering. A schematic of the austempering process is shown in Figure 15 and an illustration of the microstructural evolution at each stage is given in Figure 16.

The initial as-cast microstructure consists of graphite nodules surrounded by ferrite rings with pearlite making up the rest of the microstructure. During the austenitizing step, the microstructure consists of graphite nodules and austenite which is enriched with carbon from the now dissolved pearlite. Following the quench into the molten salt bath, ferrite begins to form while carbon partitions into the austenite. After holding at this temperature for a time, the final structure consists of graphite nodules with fine ferrite and austenite called ausferrite. This final microstructure is extremely strong and tough due to the fine ferrite and retained austenite which effectively impedes the motion of dislocations.

The final microstructure of the post heat treatment material is shown in Figure 17. The microstructure shows a fine dispersion of austenite (light etching) and ferrite (dark etching) and highly spheroidized graphite, which is ideal.

Hardness measurements were taken to compare the pre and post heat treatment conditions. The pre-heat treatment hardness was 88 ± 2 (95% CL) and the post heat treatment 111.2 ± 0.8. This post heat treatment hardness is equivalent to around 38-40 HRC or 1200 Mpa which is exactly the anticipated strength for a grade 3 ADI.

Finishing

Final detailing of the axes was done through a mix of forging, electroplating and painting.

Forging

Small forgings were crafted for the handless ax. A belt hook was hand-forged from a low carbon steel strip. A heart-shaped spear point was forged from 8630 steel bar stock. These parts were then finished by grinding and sandblasting in preparation for electroplating.

Electroplating

The axes were originally intended to be electroplated with copper. However, we were unable to prevent the electroplated copper from flaking off. Because of this we opted to plate with zinc instead.

We used zinc sulphate salt in a large water bath. The PH hovered between 3 and 4, which is ideal for plating. Immediately prior to electroplating, axes were sandblasted to remove surface oxides. A zinc ingot was used as a cathode to replenish the bath with zinc as plating occurred. A small power supply was used with a voltage of 3V, the amperage was not controlled and varied between 2-5A. The electroplating setup is shown in Figure 18 and the final electroplated parts including the forged belt hook and spear point are shown in Figure 19.

Handling, Painting and Staining

Handles were made from dried ironwood trees grown in the Upper Peninsula of Michigan. A single-piece handle was produced for the handle-less ax and a two piece handle was made for the handled ax. The handles were secured using gorilla glue; for the handle-less ax the spear point was also used as a wedge. Handles were stained using a medium-dark wood stain. All of the prominent heart features were painted using bright-red tractor paint, which gave the final product a strong accent. The finished axes are shown in Figure 20.

While both axes are mechanically sound and aesthetically pleasing, the team elected to send the ax with the integrally cast handle. This is because it is a single-piece casting and therefore makes better use of the casting process.

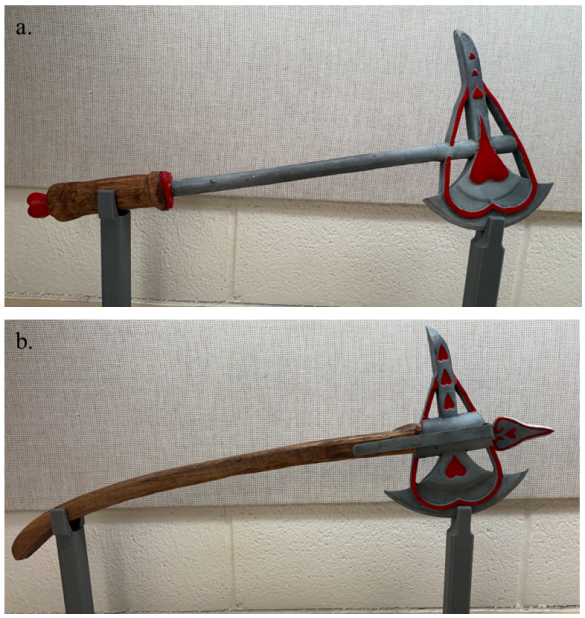

Figure 20. Final axes; integrally cast handle (top), and wooden handle (bottom).

Conclusion

The final horseman's ax successfully meets the competition requirements in both geometry and performance. The selected ADI material provided a combination of strength, toughness, and castability that enabled the production of complex features while maintaining structural integrity. The integrally cast handle design was selected as the final submission due to its efficient use of the casting process and overall robustness.

The final ax weighs 3.2 lbs and has an overall length of 22 inches, placing it within the required competition specifications. The combination of material selection, casting design, and heat treatment resulted in a functional and aesthetically distinct component that is expected to perform well in service.

Appendices

Appendix A. List of past and present horseman's axes with length width and weight

Ax type	Length (in)	Width (in)	Weight (lb)	Product or historical
Medieval horseman ax	19.5	6.2	1.75	Product
Horseman's Ax	27.7	N.A.	N.A.	Historical
Gothic Horseman's Ax	20	10	3	Product
Horseman's Ax (Czekan or Czákan)	30.75	10.75	3	Historical
Horseman's Ax	22.4	7.5	0.75	Historical
Arms & Armor Horseman's Ax	23.25	8.5	3.1	Product

Appendix B. Tables and Figures

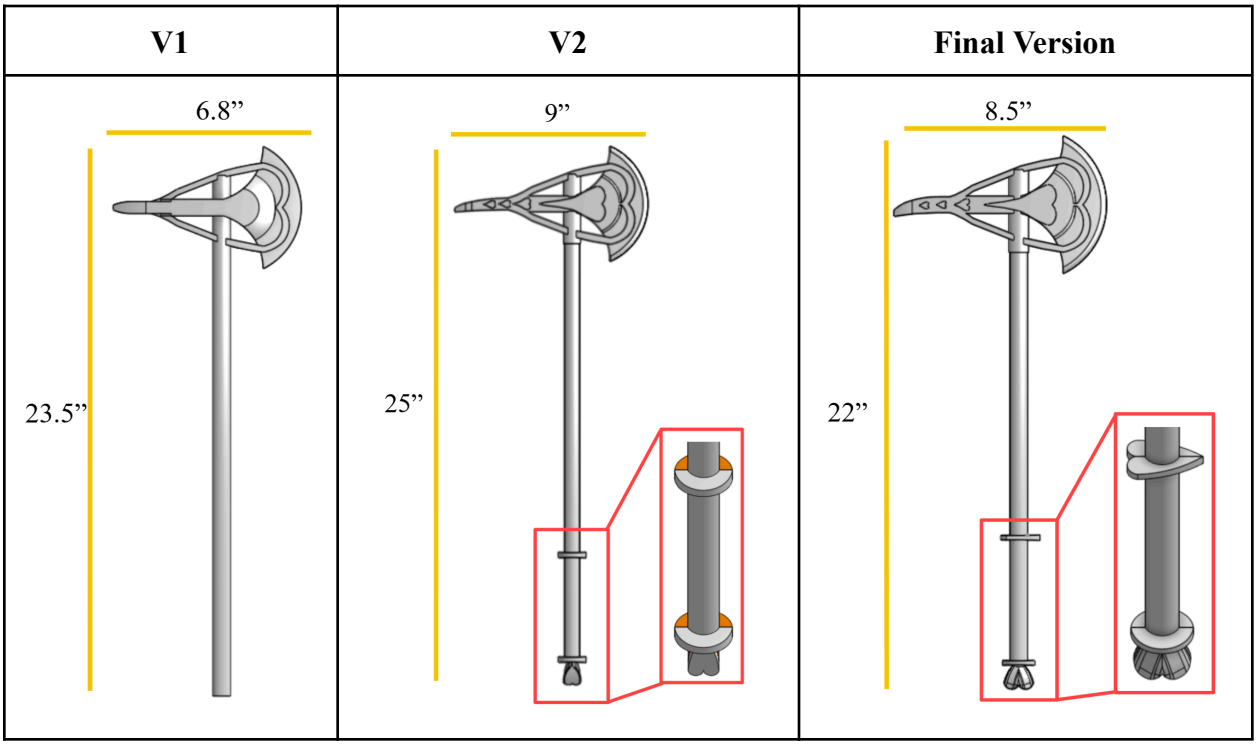

Figure 1. Design iterations of handled ax

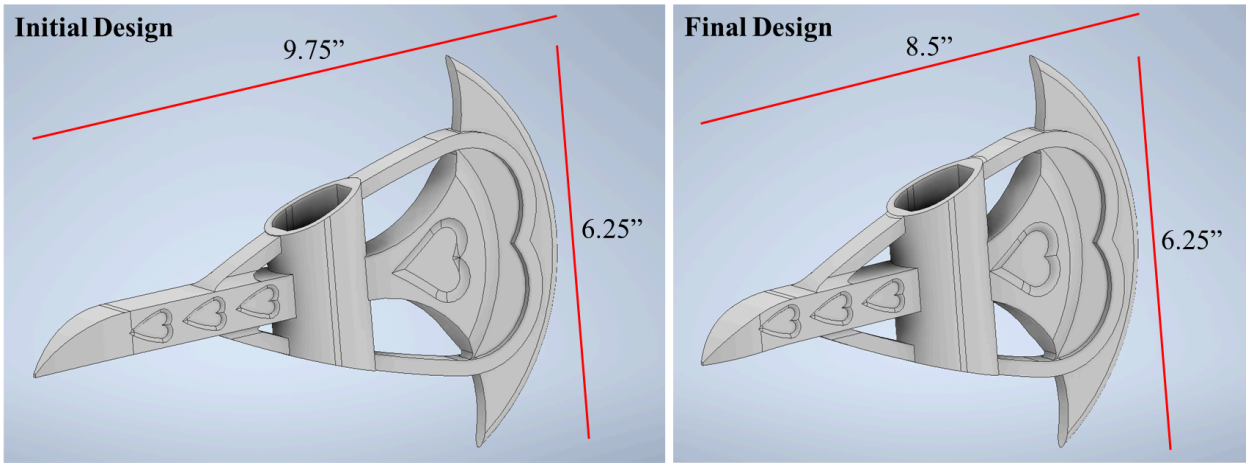

Figure 2. Design iterations of handle-less ax

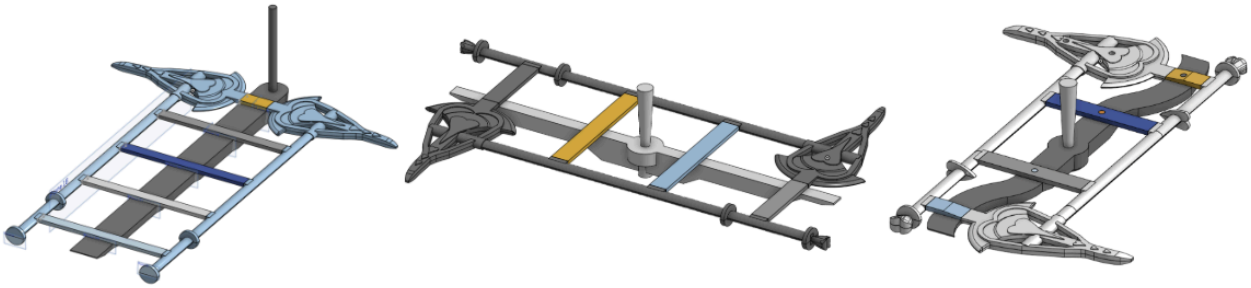

Figure 3. The three revisions of the handled ax casting design

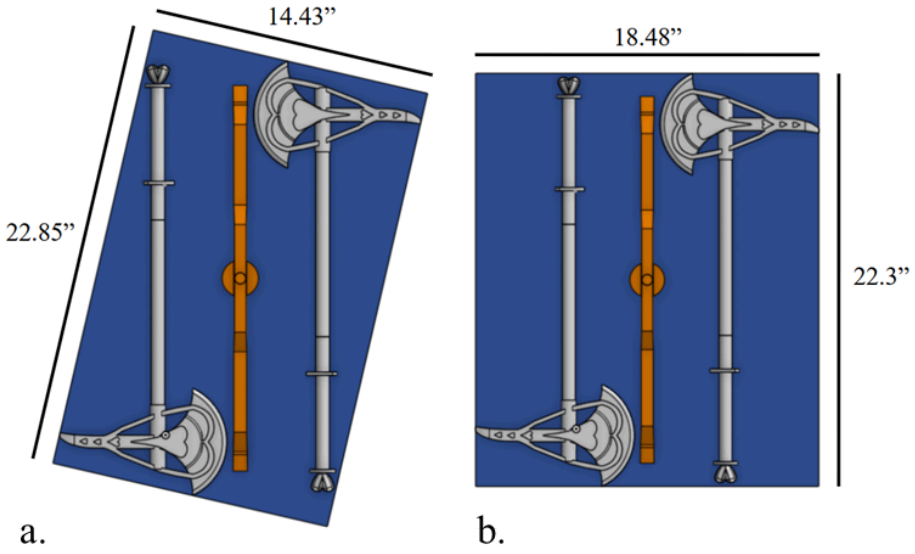

Figure 4. Rotated (a) and unrotated (b) matchplate assembly.

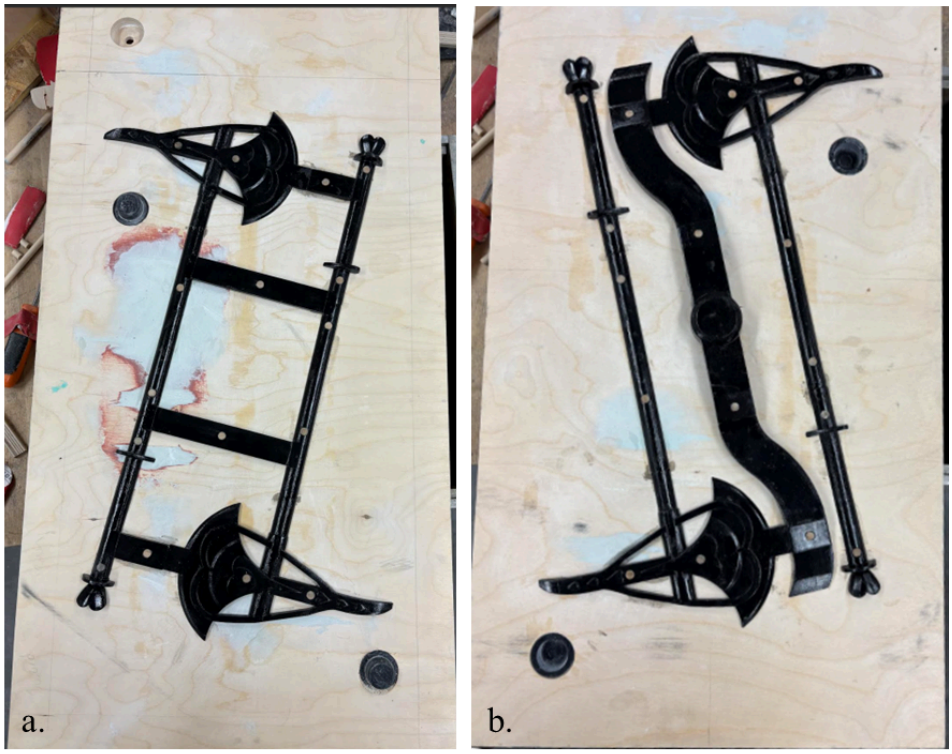

Figure 5. Handled ax pattern with the cope (a) and drag (b).

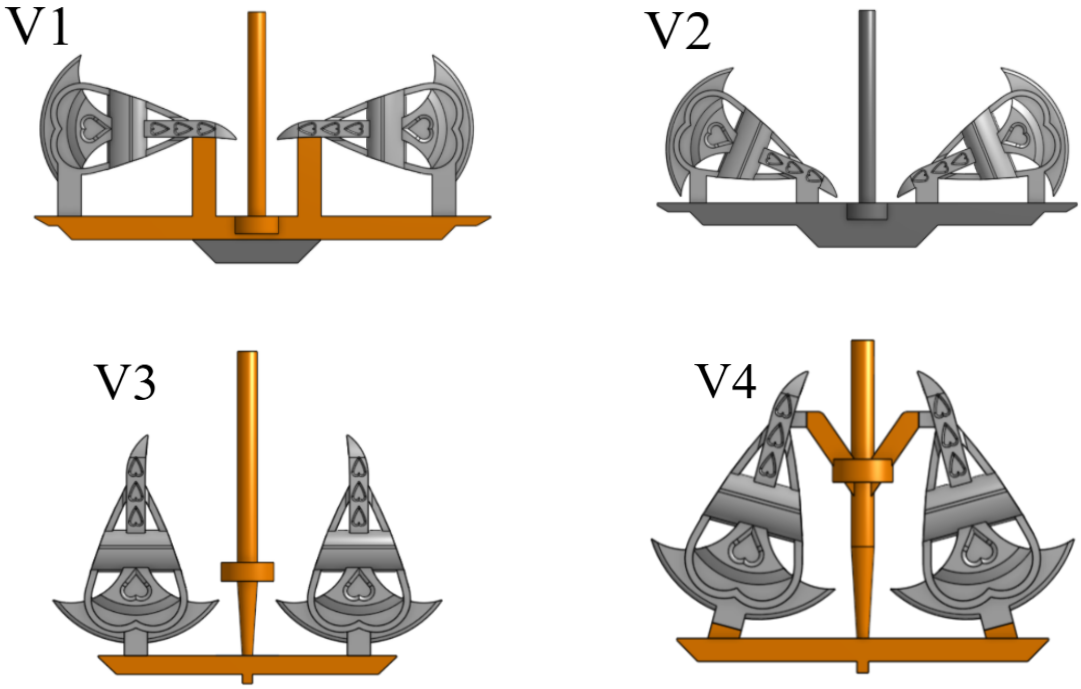

Figure 6. Design iterations for handle-less ax.

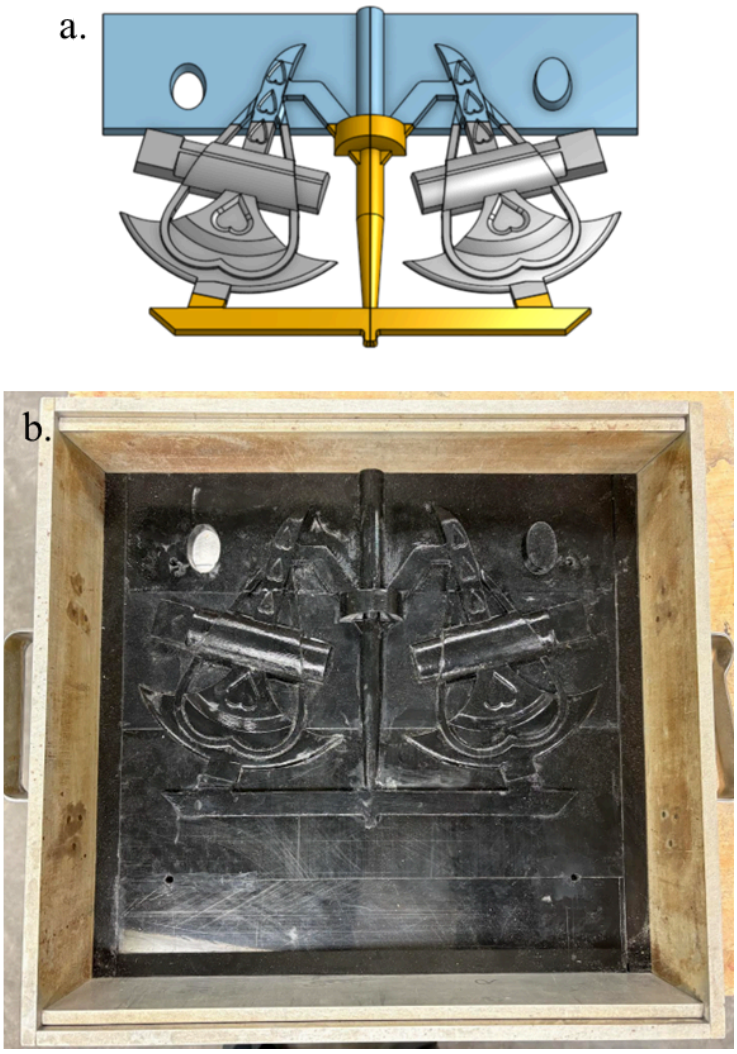

Figure 7. Final handle-less print-ready CAD (a) and final pattern (b).

Figure 8. Finished drag (a) and cope (b) molds of handled axe, along with mold for handle-less axe (c) before casting.

Figure 9. 50 lbs induction furnace used for casting.

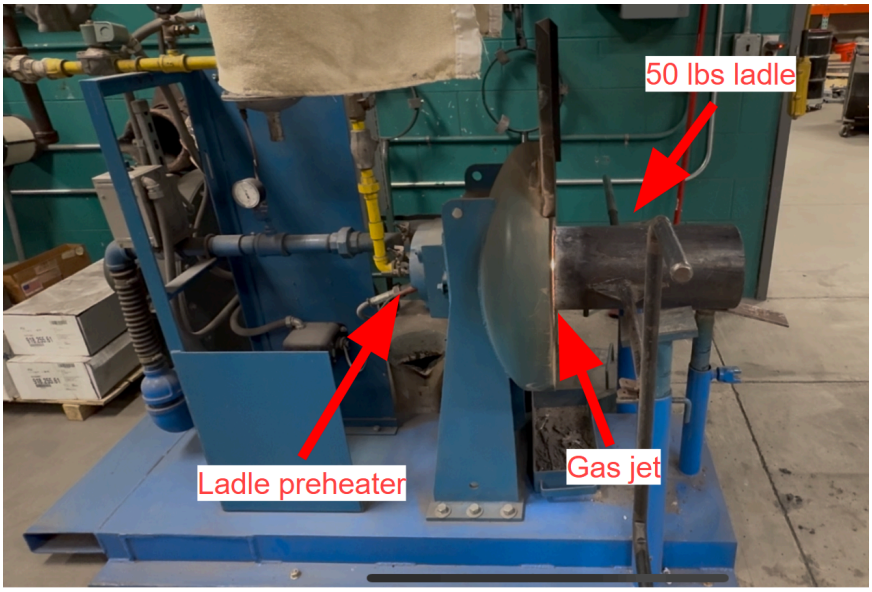

Figure 10. Ladle heater used prior to casting.

Figure 11. Post-breakout results of casting.

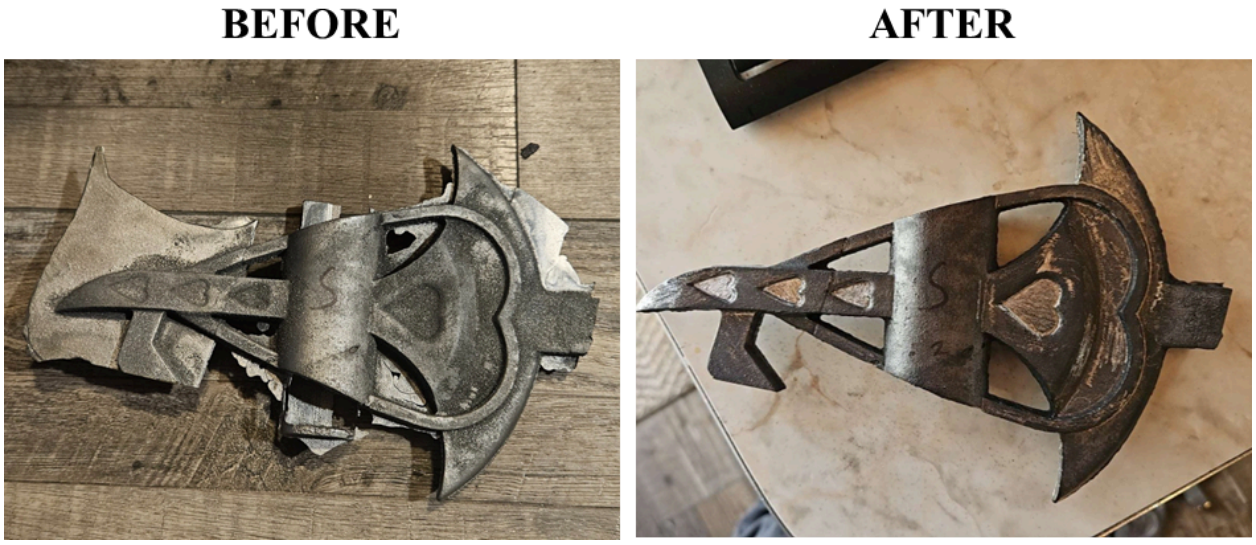

Figure 12. Example of handle-less ax before and after the fettling process.

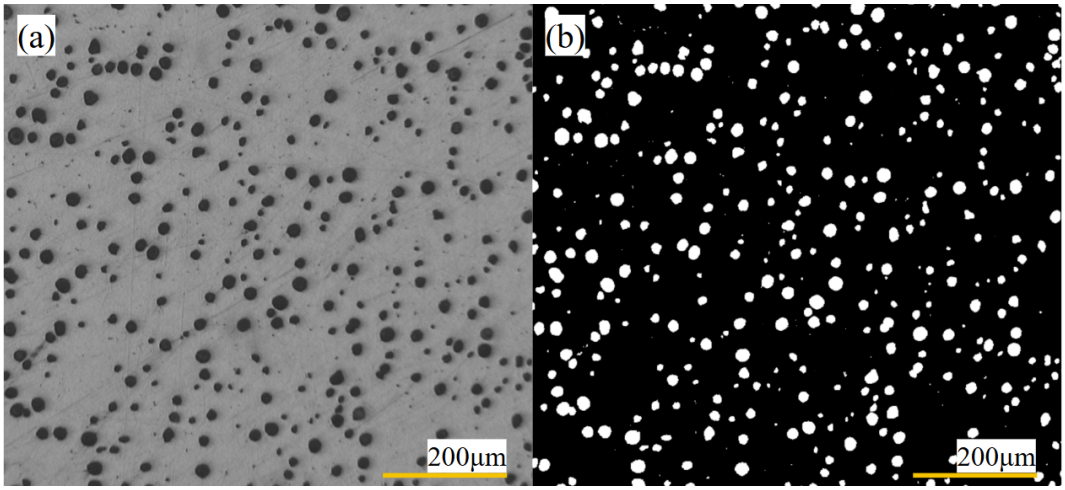

Figure 13. Polished surface of cast iron (a), the same image after undergoing thresholding using ImageJ (b).

Table 1. Nodularity, area fraction and equivalent diameter of graphite; 95% CL given; n = 9

Method	Sample	Nodularity (%)	Graphite Area Fraction (%)	Avg. Equivalent Diameter (µm)
ImageJ Manual Thresholding	**Handled A**	76 ± 2	16.7 ± 1	16.1 ± 0.8
	Handled B	90 ± 2	13.4 ± 0.6	14.9 ± 0.7
	Handle-less	92 ± 3	9.5 ± 0.9	13.1 ± 0.7
ChatGPT Image Analysis	**Handled A**	76 ± 1	21.8 ± 0.5	22.0 ± 0.2
	Handled B	85.4 ± 0.8	14.6 ± 0.5	19.0 ± 0.8
	Handle-less	92 ± 2	10.2 ± 0.5	17.5 ± 0.7

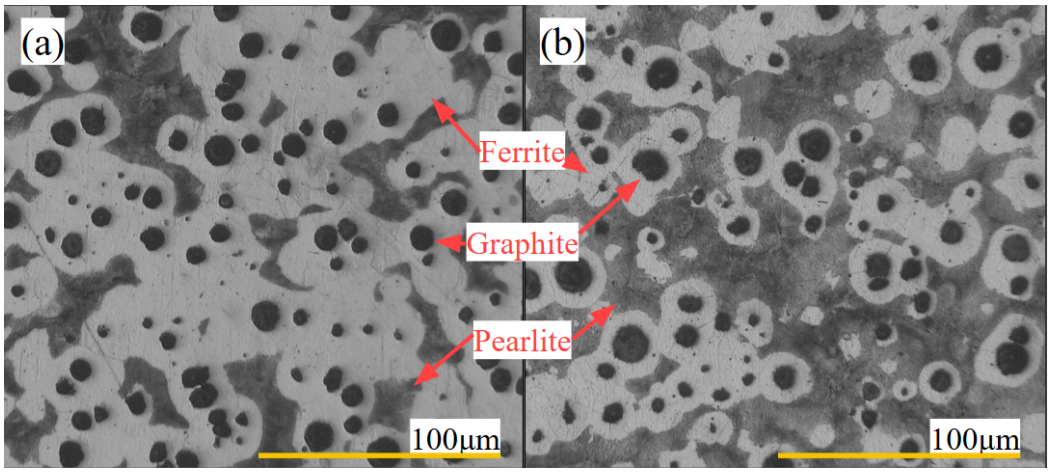

Figure 14. As-cast microstructures of: handled-ax (a) and handle-less ax (b); microconstituents are labeled. Both samples were etched with 2% Nital

Table 2. Composition target and result of as-cast B and handle-less axes 95% CL given with n=3

Element	C	Si	Mn	Cu	Mg	P	Sn
Target	3.6	2.5	0.302	0.254	0.04	< 0.05	< 0.05
Measured	3.289 ± 0.03	2.76 ± 0.04	0.323 ± 0.005	0.077 ± 0.001	0.026 ± 0.001	0.024 ± 0.001	0.003 ± 0.001

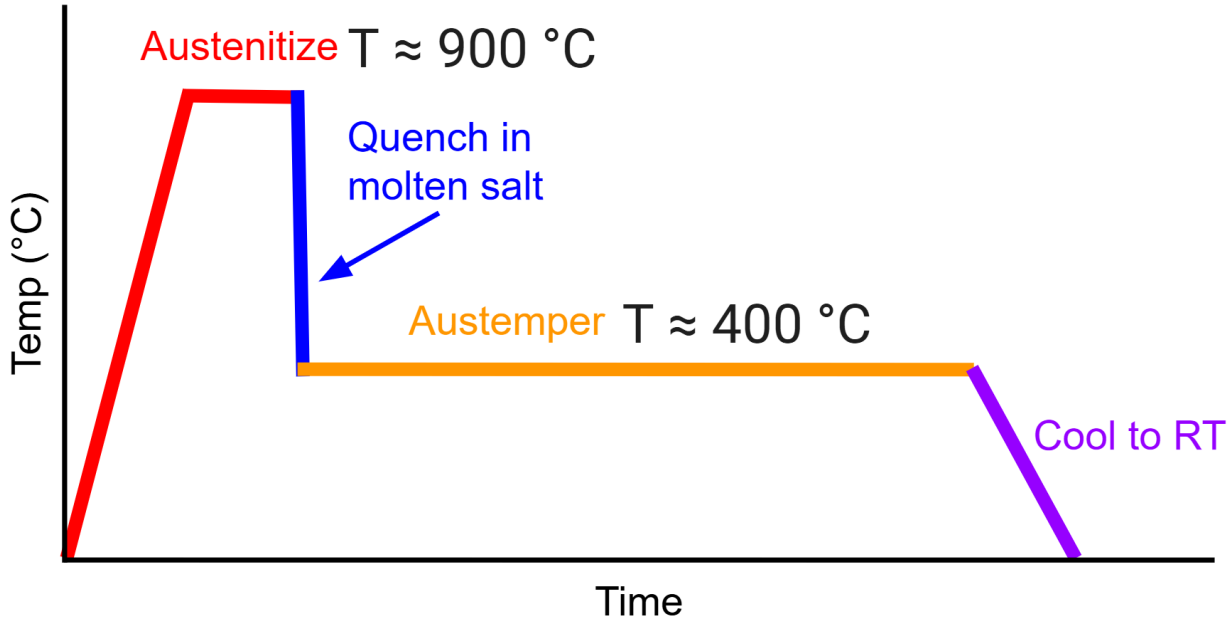

Figure 15. Schematic diagram of austempering heat treatment.

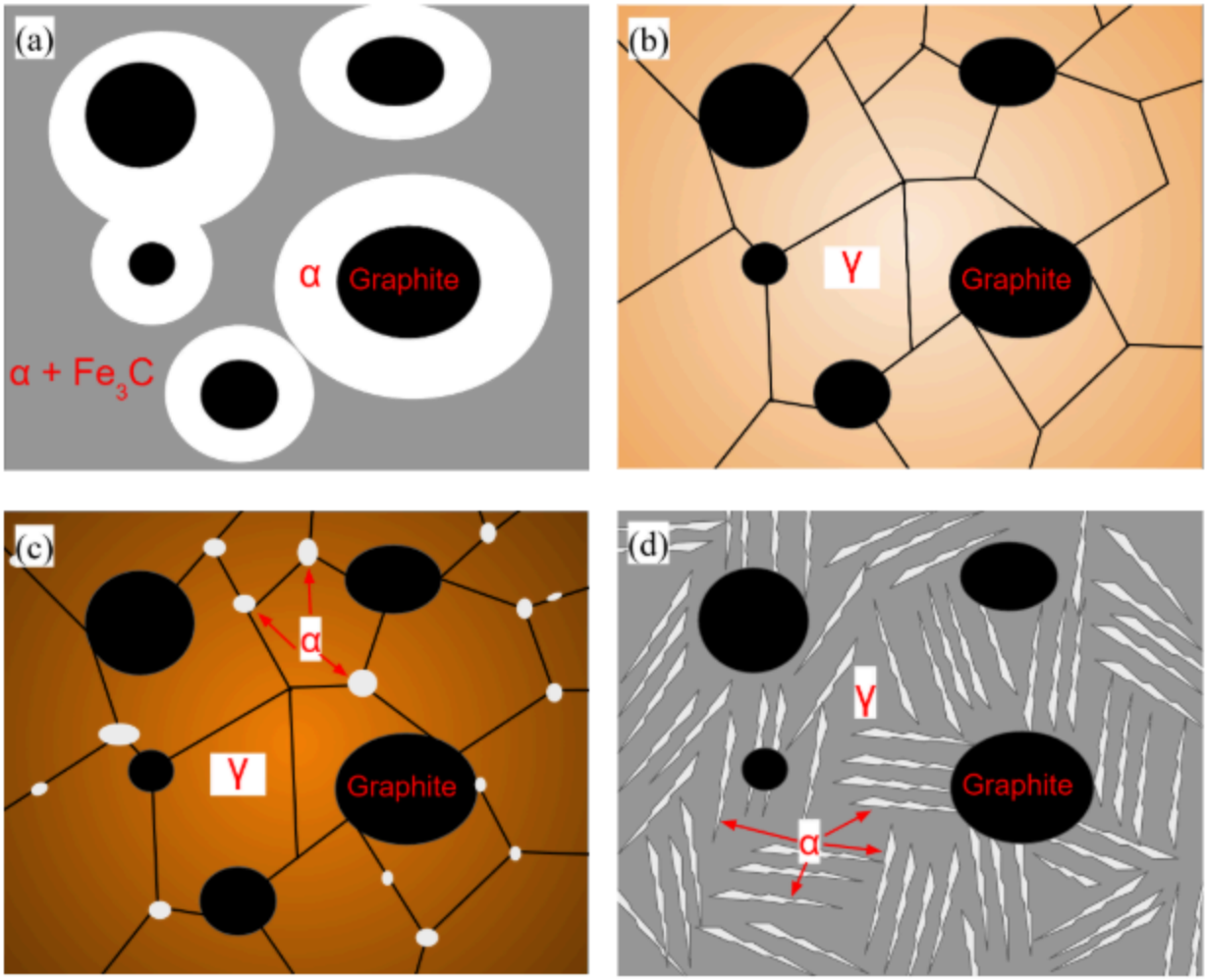

Figure 16. Microstructures at different stages of the austempering process: as cast (a), austenitizing (b), immediately following molten salt quench (c), final microstructure (d).

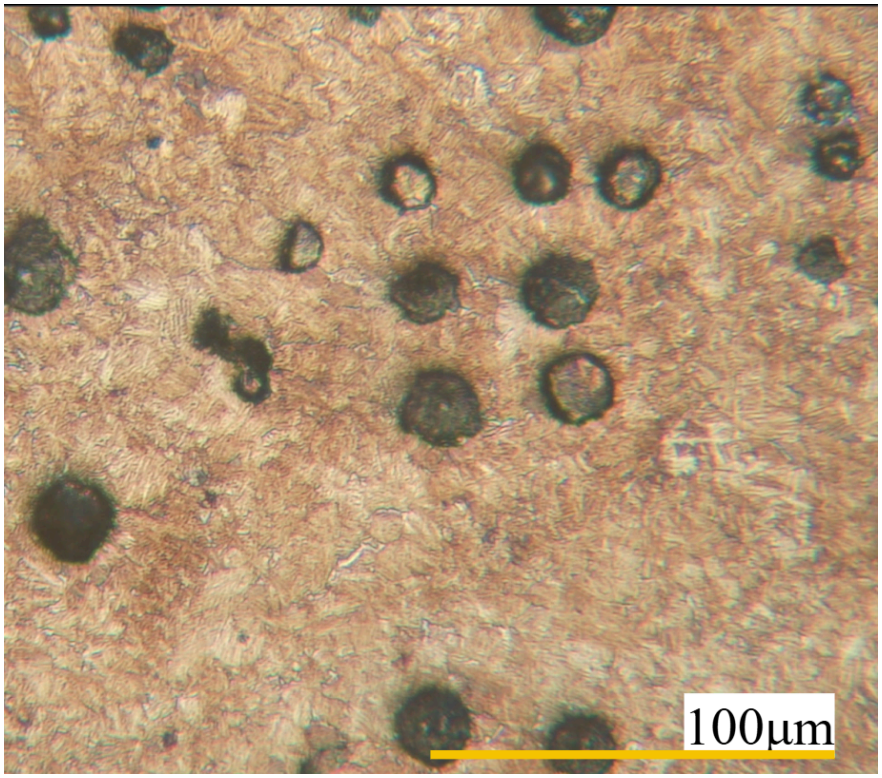

Figure 17. Final post heat treatment microstructure; the sample was etched with 2% Nital.

Figure 18. Zinc sulphate electroplating setup.

Figure 19. Final electroplated axes, belt hook, and point.

Appendix C. Charge sheet for casting

A	B	C	D	E	F	G	H	I	J	K	L	M	N	O	P	Q	R	S	T	U	V
D260206	80-100-03 Ductile	Heat 1				Notes	Horseman's axe w/ handle														
							Horseman's axe heads														
Assumptions	Charge	Top					tensile bars														
Si Recovery	0.995	0.99																			
C Recovery	0.99	0.96																			
Ladle Si recovery	0.98	0.9																			
Mg recovery	0.5																				
		Mg Required	0.75*%S + 0.025 =		0.0294566802ℇ																
Targets	Comp	CE	C	Si	Mg	Mn	P	S	Cu	Cr	Mo	Ni	Al	Nb	Co	V	Ti	W	Zn	B	Pb
	Lower	4.18	3.40	2.35		0.28	0	0.003	0.28	0.00											
	Target	4.44	3.60	2.50		0.30	0.02	0.008	0.30	0.00											
	Upper	4.71	3.80	2.70		0.33	0.03	0.020	0.33	0.10	0.01	0.20	0.050		0.03						0.008
	Material	Weight (lbs)	C	Si	Mg	Mn	P	S	Cu	Cr	Mo	Ni	Al	Nb	Co	V	Ti	W	Zn	B	Pb
Furnace Additions	Steel Punchings-32444		0.067	0.075		0.23	0.013	0.007	0.075	0.041	0.012	0.029	0.015	0.0057	0.0053	0.0017	0.0006	0.0089	0.0005	0.0004	0.012
	Steel Punchings-33757	9.00	0.179	0.152		0.59	0.0065	0.0055	0.086	0.065	0.016	0.046	0.047	0.0047	0.007	0.0025	0.017			0.0010	
	Pig Iron -Neenah		4.35	0.12		0.010	0.017	0.013	0.016	0.036		0.053	0.003		0.036	0.038	0.037				
	Waupaca Sep17 risers		3.7	2.50		0.29	0.031	0.004	0.12	0.174		0.022	0.022				0.006				
	Waupaca Mar22 Risers	29.00	3.69	2.56		0.28	0.024	0.004	0.21	0.03	0.007	0.037	0.012	0.002	0.003	0.006	0.010			0.0001	0.001
	Pig Iron Waupaca	13.0	4.56	0.025		0.01	0.0403	0.010	0.0034	0.001	0.0005	0.0064	0.007							0.0001	
	FeMn (HW)	0.030	6.38	0.47		76.28	0.185	0.01													
	D230815 Pig		3.74	1.50		0.277	0.01	0.012	0.617	0.039	0.0038	0.041	0.016	0.0036	0.013	0.011	0.004	0.0066			
	Cu Scrap	0.065							99.7												
	75%FeSi Febasa Std Grd			75.4		0.38	0.024	0.002		0.22			0.52				0.04				
	Desulco 9001	0.325	99.7					0.03													
	Furnace Weight	51.42	3.841	1.470	0.0000	0.3078	0.0250	0.0059	0.2604	0.0285	0.0069	0.0305	0.0168	0.0020	0.0029	0.0038	0.0086	0.0000	0.0000	0.0003	0.0006
			CE =	4.33																	
Ladle Additions	HW - 5LB MgFeSi	0.8		45.66	6.0600								0.930								
	R6-12 GloMag			46.17	6.8000								0.850								
	Alinoc 65			65.00									3.000								
	Ultraseed Ce			73.07									0.870								
	Topseed	0.25	0.094	49.04									1.038								
	Cover Steel - thin	0.3	0.067	0.019		0.492	0.0044	0.0063	0.027	0.023	0.002	0.012	0.037	0.0023	0.0035		0.0012	0.014			0.0069
	Steel Punchings-28843		0.098	0.028		0.40	0.012	0.007	0.096	0.064	0.011	0.029	0.040	0.0046	0.0032	0.0025	0.0038	0.012	0.0015		0.012
	Treated Total	52.77	3.744	2.338	0.0459	0.3027	0.0244	0.0058	0.254	0.028	0.0067	0.0298	0.0356	0.0019	0.0029	0.0037	0.0084	0.0001	0.0000	0.0003	0.0006
		Percent	CE =	4.53																	
Mold or In-Stream Inoculants	Foundrisil 75	0.25%		75.70									0.990								
	Elkem Superseed 75			75.15				0.04					0.26								
	Final Composition	**52.90**	**3.734**	**2.502**	**0.0458**	**0.302**	**0.024**	**0.006**	**0.253**	**0.028**	**0.007**	**0.030**	**0.038**	**0.002**	**0.003**	**0.004**	**0.008**	**0.000**	**0.0000**	**0.0003**	**0.001**
			CE =	4.57																	
		CE	C	Si	Mg	Mn	P	S	Cu	Cr	Mo	Ni	Al	Nb	Co	V	Ti	W	Zn	B	Pb
	Target Difference	0.02	0.0940	-0.1618	0.0000	0.0000	0.0000	0.0000	0.0000	0.0000	0.0000	0.0000	1.0380	0.0000	0.0000	0.0000	0.0000	0.0000	0.0000	0.0000	0.0000
	Analysis Totals -	base 1																			
		base2																			
		final																			
Instream Weight	52.77	(lbs)																			
	Foundrisil 75	0.131925		59.89 grams																	
Inoculate per Mold	Elkem Superseed 75	0																			
Carbon Loss Factor for final ramp to 1500C			0.08-0.10%																		

Appendix D. ChatGPT Prompt for Image Analysis for ChatGPT 5.2

You are provided a set of unetched cast iron microstructure images. Perform automated graphite image analysis using the following fixed pipeline and do not deviate from it. Convert each image to grayscale. Apply flat-field correction by creating a background using a large Gaussian blur with sigma approximately 25 pixels and normalize the original grayscale image by this background such that the mean intensity is preserved. Apply a mild Gaussian blur with a 5×5 kernel. Perform per-image Otsu thresholding using a binary inverted threshold. Apply morphological opening with a 3×3 elliptical kernel for one iteration, followed by morphological closing with a 5×5 elliptical kernel for one iteration. Detect external contours only. For each contour compute area A, perimeter P, circularity defined as $4\pi A/P^2$, and equivalent circle diameter defined as $\sqrt{(4A/\pi)}$. Apply particle filtering such that any particle with area less than 150 px^2 is rejected and any particle with circularity less than 0.10 is rejected. Define nodules as particles with circularity greater than or equal to 0.65. For each image calculate nodularity (%) as the number of nodules divided by the total number of accepted particles times 100, graphite area fraction (%) as the sum of accepted particle areas divided by total image area times 100, and average equivalent diameter from accepted particles. Use a scale conversion of 200 μm corresponding to 292.11 pixels (0.6847 μm per pixel) to convert average diameters to micrometers. Treat each image as one independent sample. Report the mean and 95% confidence limit for nodularity, graphite area fraction, and average equivalent diameter using 95% CL = $\pm 1.96 \times$ (sample standard deviation / $\sqrt{n}$). Output a table of per-image results followed by a table of group means with 95% confidence limits. Do not tune parameters to match expected values, do not use adaptive thresholding, and do not manually edit images.